arXiv:1403.7445v2 [cond-mat.mtrl-sci] 31 Mar 2014

A Combined Structural Analysis Refinement of a Strained $LaVO_3$ Thin Films

H. Rotella, O. Copie, P. Boullay, H. Ouerdanne, A. David, A. Pautrat, D. Chateigner, and W. Prellier*

Laboratoire CRISMAT, CNRS-ENSICAEN and Universite de Caen Basse Normandie (UMR 6508), 6 boulevard du Marechal Juin, 14050 Caen Cedex, France

P. Roussel

Laboratoire UCCS, CNRS UMR 8181, ENSCL, Bat C7, BP 90108 F-59652 Villeneuve dÕAscq, France.

M. Morales

CIMAP, CNRS-ENSICAEN and Universite de Caen Basse Normandie (UMR 6552), 6 boulevard du Marechal Juin, 14050 Caen Cedex, France

L. Lutteroti

Dipartimento di Ingegneria dei Materiali, Univ. di Trento, I-38050 Trento, Italy.

Abstract

While the structure refinement has become straightforward for simple bulk material, the accurate structural determination is still challenging for thin film. Using a combined analysis approach, we have investigated the crystal structure of $LaVO_3$ thin films grown on (001)-oriented $SrTiO_3$ substrate. Transmission electron microscopy reveals that the thin films are epitaxially grown on $SrTiO_3$ and underlines the presence of 90° oriented domains. Then, the mapping of the reciprocal space by high resolution X-ray diffraction allows to refine the lattice parameters. We deduce that the strain accommodation imposes a monoclinic structure. The reciprocal space maps were then processed and the extracted data computed to refine the atomic positions. We discuss the obtained results and our methodological approach as a promising thin film structure determination for complex systems.

PACS numbers:

*wilfrid.prellier@ensicaen.fr

I. INTRODUCTION

Transition metal oxides (TMOs) have been fascinating for many years due to their broad spectra of functional properties, such as metal-insulator transition, ferroelectricity, superconductivity, colossal magnetoresistance etc.[1–6] Compared to semiconductors or metals, interactions, such as Coulomb repulsion, compete each other in TMOs, giving rise to strong coupling between lattice, charges, spins and orbitals.[7] Among the oxide compounds, Mott insulator [8] are a typical example of the competition between kinetic energy and Coulomb repulsion that induces an insulating behavior. Besides, the lattice structure is also an important parameter governing the electron transport that influences the metal-to-insulator transition. Furthermore, these materials are very sensitive to external stimuli such as temperature or hydrostatic pressure. Thus, taking advantage of the substrate induced biaxial strain, the thin film deposition provides a way to tune the TMOs properties.[2–4, 6, 9] As an example, octahedral rotations in ABO_3 compounds affect directly the orbital overlaps trough the B-O-B angles and could modify transport properties. The majority of the perovskite group compounds are distorted derivatives of the parent cubic ($Pm\bar{3}m$ (#221)) resulting from a combination of the contributions : (i) tilting of BO_6 octahedra; (ii) Jahn-Teller distortion of BO_6 octahedra; (iii) cation displacement. Several theoretical studies have already addressed the crucial role of those contributions on electronic properties.[7]

As, the control of the properties of these systems is extremely important in view of their potential technological perspectives, it becomes crucial to understand accurately the structure. While many improvements have been made in the synthesis of perovskite thin film and complex heterostructures, little is known about the crystal structure. It becomes thus difficult to quantify, in a thin film, the relationships between physical properties and lattice structure. Here we present the experimental study of the oxide thin film structure by the combined analysis using X-ray diffraction measurements. X-rays diffraction (XRD) is still after a century, the mostly used non-destructive analytical techniques which reveals informations about the crystal structure.

Using Rietveld's method, many bulk structures have been resolved from powder diffraction analysis. However, in peculiar cases the grinding could be unacceptable, think of thin film heterostructure, where the grinding will destroy the material and the properties. Thus, the as-studied powder could not be compare to the parent sample. In addition, when the

film thickness decreases drastically, the amount of studied phase is negligible with respect to the substrate contribution. To avoid such difficulty, the combined analysis method has been developed.[10] This technique is based on the Rietveld's method in which a texture parameter is added to the intensity formula. This non-destructive technique can further quantitatively determine the referred orientations, structure, crystal sizes, phases while the sample remains intact. With the development of this method, and the constant improvement in the XRD apparatus (more intense sources (rotative anodes), experimental set-up with seven-circles diffractometers...), the structural analysis of thin films has successfully already been resolved.[11–14] The considered systems were either the film and the substrate are not isostructural or the film is not fully textured or epitaxially grown on the substrate.

However when comes the question of complex systems structural analysis like epitaxial oxide thin film grown on an isostructural substrate, the accurate structure refinement is still challenging. Firstly, the epitaxy of the film produced a highly textured material which often presents oriented crystallographic domains. It results on a complex diffracted pattern with the convolution of several cristallographic planes contribution in one peculiar reflection. Secondly, the isostructural relation between the film and the substrate structure produced two diffracted patterns in the reciprocal space which are very close one from the other. The amount of substrate material being 5 order of magnitude higher than the film one, the diffracted beam coming from the substrate is more intense than the film signal and, if the structures are close, the substrate signal can modify the film signal. The deconvolution of the two signals becomes, thus, difficult. Thirdly, the thin thickness (100 nm) of the film produces a weak diffracted beam. It can results in the extinction of the weak reflections in the diffracted pattern which should normally be present because of the peculiar film structure. In addition to those sample constrains in the study, the experimental set-up itself produces limitations in the data acquisition. The system film+substrate allows us to be only in the reflection configuration. In this specific configuration, the experimental set-up produces shadow zones in the diffracted pattern, resulting in inaccessible reflections.[15]

The solution to overrule these constrains is to combined several techniques and to separate the analysis in several focus points. Firstly the combination of transmission electron microscopy (TEM) and XRD analyses results in a complete knowledge of the film structure. Secondly, a film structure analysis can be realized by separately focusing on the epitaxial relations between the film and the substrate, on the refinement of the lattice parameters

of the film, even the determination of the atomic position can be separate by focusing on a peculiar kind of atoms. Especially in the case of oxide perovskite compounds, it as been proved that the displacements, from the ideal positions, of the oxygen atoms produce specific reflections in the diffracted pattern.[16, 17]

Recently partial structural studies focused on the distortion of the structure and the oxygen atomic positions have been reported.[18–21] The different studied systems present oxygen octahedral tilt system in bulk form. In order to accommodate the substrate induced strain, oxygen octahedral tilt system in the film is modified, resulting in a distortion of the crystal structure with respect to the bulk one. The B-O-B angles is changed as well as the orbital overlapping. The determination of the octahedral rotations opens the route towards the determination of the orbital interactions and the improvement of the accurate understanding of the observed physical properties.

Here we focus on the characterization of the structure of $LaVO_3$ (LVO) thin films grown on (001)-oriented $SrTiO_3$ substrates. In its bulk form, LVO crystallizes at room temperature in an orthorhombic structure ($Pnma$ (#62)) with the following lattice parameters, a_o=5.5529(2) Å, b_o=7.8447(3) Å and c_o=5.5529(3) Å .[22] LVO structure presents mostly tilting of BO_6 octahedra and La displacements which makes it derivate from the parent cubic structure ($Pm\bar{3}m$ (#221)). However in the case of LVO those distortions are relatively small and the lattice parameters can be related to a pseudocubic one according to the following equation : $a_p \simeq a_o/\sqrt{2} \simeq b_o/2 \simeq c_o/\sqrt{2} \simeq 3.9251(1)$ Å. The mismatch between $a_{p_{LVO}}$ and a_{STO} is about 0.5% indicating a compressive stress. Previously, we have shown that $LaVO_3$ film grown on $SrTiO_3$ substrate adopts a distorted orthorhombic structure with the long axis in the substrate's plane. By assuming the oxygen octahedra as rigid body we evaluated the tilt system in LVO thin film to be (a^- a^+ c^-) with $\alpha = \beta \simeq 3.1(1.7)^\circ$ and $\gamma \simeq 11.3(1.8)^\circ$.[19, 23] In this article, we extend our study using a combined XRD analysis and resolve the structure of epitaxial $LaVO_3$ thin films. On one hand we further succeeded in the cell parameters refinement. On the other hand we achieved first results on the atomic positions.

II. EXPERIMENTAL

A. Synthesis

Epitaxial $LaVO_3$ (LVO) thin films were grown by pulsed laser deposition technique on (001)-oriented $SrTiO_3$ (STO) substrate (cubic a=3.905 Å). To grow the film, a KrF laser (λ=248 nm) with a repetition rate of 2 Hz and a fluence of $\simeq$ 2J/cm^2 was focused onto a $LaVO_4$ polycrystalline target. The substrate is kept at 700°C under a dynamic vacuum around 10^{-5} mbar. The distance between the target and the substrate is 8.5 cm.[24, 25]

B. Structure analysis

Sample used for transmission electron microscopy analysis was prepared in cross-section with a dedicated JEOL ion slicer. After a hand polishing with a series of grinding paper, the cross-section is achieved using a Ar ion beam to decrease the thickness down to 100 nm. Selected-area electron diffraction (SAED) and transmission electron microscopy (TEM) images were obtained using a JEOL 2010 FEG microscope with a 2.1 Å resolution on the thin film cross-section.

The reciprocal space map (RSM) were acquired using a high resolution 4-circles diffractometer Rigaku having a copper rotative anode (λ = 1.54056 Å) and a 1D detector of 2° (at Lille, UCCS). This apparatus presents weak wavelength dispersion ($\frac{\Delta\lambda}{\lambda} = 3,8 \times 10^{-4}$) and weak beam divergence ($\Delta\omega = 32'$). The resolution is $\Delta\theta = 0.005°$ and the 1D detector records simultaneously 2° using 120 channels. For the reflexions were both the film and the substrate contributions are presents, the optimization is performed on the film.

C. Data processing

While exploring the reciprocal space, we scan several reciprocal lattice points, each one being associated to a crystal plane family. If the angles between incident ($\overrightarrow{k_i}$) and diffracted ($\overrightarrow{k_d}$) beam vectors is appropriate to be in the Bragg's diffraction conditions, a reciprocal lattice point is found at the end of a vector $\overrightarrow{q} = \overrightarrow{k_d} - \overrightarrow{k_i}$ (see the schematic representation Figure 1).

For the sake of clarity, two reference coordinate systems have to be defined to describe

the sample environment. The first reference coordinate system is the sample surface which contains the two axes $\overrightarrow{x}$ and $\overrightarrow{y}$. The $\overrightarrow{z}$ axis is consequently perpendicular direction. In this coordinates system, three sample's rotation angles χ, ω and ϕ associated to $\overrightarrow{x}$, $\overrightarrow{y}$ and $\overrightarrow{z}$, respectively are described. The fourth circle of the diffractometer corresponds to the Bragg's angle, 2θ, which is given by the detector position. The second reference coordinate system is the crystallographic orientation of the crystal in the sample described by the three vectors $\overrightarrow{a}$, $\overrightarrow{b}$, and $\overrightarrow{c}$ which are along the cell parameters.

When tilting the sample around the three x, y and z axes, the beam penetrates the sample differently, and a correction of the intensity before analysis is required as describe by the following equations :

$$I_{corr} = \frac{I_{mes}}{A_{\chi}^{film}} \tag{1}$$

where A_{χ}^{film} is the correction factor expressed by :

$$A_{\chi}^{film} = \frac{2}{\sin(2\theta)M(\omega,2\theta)} \frac{1-\exp(\frac{-\mu T M(\omega,2\theta)}{\cos(\chi)})}{1-\exp(\frac{-2\mu T}{\sin(2\theta)\cos(\chi)})} \tag{2}$$

where the factor $M(\omega, 2\theta)$ is

$$M(\omega,2\theta) = \frac{1}{\sin(2\theta)} + \frac{1}{\sin(2\omega-2\theta)}. \tag{3}$$

Once this correction applied, we can process the corrected RSM. Each RSM is made of a series of 1D diffractogrammes of 2° in ω for one 2θ fixed, represented by the (**a**) arrow on the figure 2. In order to calculate the integrated intensity, we develop a program fitting each ω scan to get an intensity for each associated 2θ value. In figure 2a we show the raw data for a ω scan at a given 2θ value. First, the data are smoothed by using the method described by Sonneveld and Visser.[26] The same algorithm is used to determined the background. Secondly the smoothed data and the background are interpolated in order to get the integrated intensities of both plot. We obtain the distribution of the intensity of the smoothed data and the background along 2° in 2θ represented by the (**b**) arrow and plotted in figure 2b). Finally, the difference between the interpolation of both distributions gives the integrated intensity value of the 3D RSM.

III. RESULTS

A. TEM investigation

Preliminary investigations were made using transmission electron microscopy (TEM) on a 200 nm-thick film. The TEM image, shown in Figure 3a, presents a thin film having a high crystalline quality. This study reveals a perfect epitaxy of the film on the substrate at the interface and a full conservation of the strain all along the thickness. The associated selected area electron diffraction performed on the film reveals that epitaxial $LaVO_3$ keeps a structure close to its bulk orthorhombic form with a slight modification of the lattice parameters to minimize the strains. But the reconstruction, represented in Figure 3c, of the diffracted pattern (Figure 3b) underlines the contribution of two 90°-oriented variants in the film, represented in Figure 3d and 3e. We can thus conclude on the orientation of the film which can be describe by the epitaxial relationships $[101]_F//[001]_S$ and $[010]_F//[100]_S$ or $[010]_F//[010]_S$ (where subscript S and F refers to the substrate and film, respectively) in agreement with previous studies on similar systems.[23]

B. Pole figure simulation

A perfect epitaxial film, i.e. without any growth defects, should be a single crystal, also named fully textured. In reality, most of the epitaxial thin film present several crystallites with different orientations. Considering one peculiar reflection hkl, we defined a pole sphere centered on the sample, where the orientations of the $\overrightarrow{q}$ vector are characterized by the angles χ and ϕ in the diffractometer space. The representation of the distribution of the orientation of one reflection is visualized using a pole figure. A pole figure of a given reflection is the Lamber projection of the pole sphere. Each point P of the pole sphere is projected at a point P' on the tangent plane at the north pole of the sphere pole (see Fig 4). The position of P' on this plane is defined by the ϕ angle value and $r' = R\sin(\chi/2)$, where R is the sphere pole radius.

In the case of $LaVO_3$ thin film, according to the TEM analysis, four 90° oriented domains are present in the sample. Using the MAUD software, the simulation of the pole figure of four reflections were performed. We focus on the 101, 020, 204 and 323 reflections. First, considering that the film is fully textured, i.e. with only one orientation described by

the relations $[101]_F//[001]_S$ and $[010]_F//[100]_S$, we simulate the four pole figures shown in figure 5. Each reflexion can clearly be observed independently from the others as well as its multiplicity. For example, the 323 reflection presents 6 equivalents, while the 204 reflection shows only 2.

Secondly , we defined in the software four orientations to represent the four 90° oriented domains of the crystal, resulting in the pole figures represented in figure 6. We considered the following orientations : $[101]_F//[001]_S$ and $[010]_F//[100]_S$ or $[010]_F//[010]_S$ or $[010]_F//[\bar{1}00]_S$ or $[010]_F//[0\bar{1}0]_S$. It clearly appears the convolution of several reflections at the same position in the pole sphere. At the equator of the pole sphere, the 101 and the 020 equivalents are mixed, as well as are the 204 and 323 equivalents near the north pole. This can be easily explained because of the very close values of the LVO lattice parameters. In conclusion, this simulation indicates that the presence of 90° oriented domains implies that some reflections in the diffracted reciprocal space can present the contribution of several crystallographic planes.

C. Cell parameters refinement

In order to invest deeper the structure of LVO in thin film form, we perform high resolution XRD measurement on a 100 nm-thick film. First, we focus on the characterization of the epitaxial relation between the film and the substrate by looking at the four asymmetric reflections (204), (402), (323) and (3-23) shown in Fig. 7. They are represented in the reciprocal lattice units q_x, q_z by using the formula 4 and 5, where λ is the wavelength and θ and ω are the angles described in figure 1.

$$q_x = \frac{2\pi}{\lambda}(\cos(2\theta - \omega) - \cos(\omega)) \tag{4}$$

$$q_z = \frac{2\pi}{\lambda}(\sin(2\theta - \omega) + \sin(\omega)) \tag{5}$$

This representation is valuable in the case of those reflections because the measurement is achieved in the coplanar configuration, i.e. the angle χ in the figure 1 is kept equal to zero. In order to reach these reflections, the angle ω is defined by the relation :

$$\omega = \theta - \chi. \tag{6}$$

Figure 7 clearly shows that $LaVO_3$ film is coherently and fully strain on the substrate because of the perfect vertical alignment between the both families of reflections of the film and the substrate respectively. This results confirms the TEM observations described above. However, the horizontal alignment of these four reflections reveals that they are equivalent, as expected from the Pf simulations shown in figure 6. Indeed, the deconvolution between the two crystallographic planes families is not possible. Nevertheless, we can conclude from this observation, first, that the a and b lattices parameter of LVO in thin film form are qualitatively very close. Secondly, the four 90° oriented domains proportions are quantitatively equal because of the equivalent measured intensity for the four reflections.

To performed the cell parameters refinement we record all the accessible reflections allowed by the diffractometer set-up (see the listed reflections in table I). Unfortunately, we observed a huge distortion of the beam imprint when the sample tilts around the x axis (when χ is different from zero). This effect leads to an important error on the absolute value in 2θ of the RSM ellipse center. This can be corrected by using an analyzer crystal in front of the detector but the intensity signal decreased by 2 orders of magnitude. Several reflections coming from the film were not reachable anymore. This explained why certain reflections in table 1 are not associated to a 2θ position.

From the list of absolute value of 2θ positions associated to hkl miller indices, we realize a refinement of the cell parameters of the $LaVO_3$ thin films using the CELREF software.[27] We have shown in a previous work that $LaVO_3$ thin film grown on $SrTiO_3$ has a distorted structure toward a monoclinic structure.[19] According to the group-subgroup theory, the only possibility in our system to be in a lower symmetry is to go from $Pnma$ to $P2_1/m$.[28] Thus, the refinement procedure was achieved by refining the bulk parameters transposed in a monoclinic subcell, with the measured data performed on the film (see results in table 1). We confirm that the LVO film crystallized in a monoclinic structure, as expected. The monoclinic angle is $\beta = 89.45(9)°$ and the lattice parameters are $a = 5.554(3)$ Å, $b = 7.810(4)$ Å and $c = 5.555(5)$ Å. The b parameter verifies the relation $b = 7.810(4)$ Å$= 2 \times 3.905$ Å , confirming that the film is fully strained. This quantitative result is coherent with previous qualitative observations.[19] Comparing the bulk values with the refined ones, the a and c parameters stay equal to the bulk ones with respect to our experimental accuracy. But in order to accommodate the substrate strain along the direction $10\bar{1}$ and $\bar{1}01$ the angle β between a and c became smaller than 90°. Whereas the b parameter change significantly in

order to accommodate the substrate strain. The strain is evaluated to be $\epsilon_2 = b_B - b/b_B = 0.5\%$, where b is the evaluated value in this work and b_B is the bulk parameter. According to this refinement, the LVO thin film structure adopts a monoclinic space group which can be describe with the $P2_1/m$ symmetry.

IV. DISCUSSION.

To go further in the $LaVO_3$ thin film structure analysis, perfectly defined the space group and characterized the crystal, we focus our interest on the atomic positions determination. In fact, besides the absolute 2θ value of a RSM ellipse center, the integrated intensity measured of a reflection i is directly related to the atomic positions, through the structural factor F_k, and the orientation. The purpose in this work is to refine the atomic position of the LVO bulk compound determined by Bordet *et al.*[22] using the integrated intensity of the measured RSM on the LVO thin film. The atomic positions in the bulk compound are described in an orthorhombic space group. With the cell parameters refinement presented above we have shown that the structure of LVO thin film adopts a monoclinic space group. Using the TRANSTRU software we translate the bulk orthorhombic atomic position into a monoclinic subcell description(see results in table 3 left side).[29] The transformation creates new atomic sites corresponding to a monoclinic description (La(2), V(2), O1(2) and O2(2)). According to this new description of the crystal, it appears that 14 atomic parameters are variable, with the scale factor and the thermal agitation factors (1 per atom), there are 23 parameters to refine.

During the measurement, we observed an important distortion of the diffracted beam when recording reflection in a non-coplanar configuration (i.e. $\chi \neq 0$), but considering the very few number of accessible reflections, we assume that the integrated intensity is not influenced by the distortion of the beam when titling the sample around the x-axis. Thus, the reciprocal space maps in coplanar ($\chi = 0$) and non-coplanar configurations are investigated to get the maximum number of reflections. The limitations are the beam imprint on the sample and the diffracted intensity. Indeed, since we compare the diffracted intensity between different reflections, the incident intensity on the sample needs to be constant independently of the orientation of the sample with respect to the incident beam. Consequently, it is not possible to access reflections with small ω and high χ values.

We reported 26 measured integrated intensity. In order to performed the atomic position refinement we used the JANA2006 software.[30] This software required at least 5 more times measured intensities than the number of parameters to refine. To overcome this constrain, because of the structure of the perovskite compound, it is well known that the bond between the oxygen atoms are strong and the octahedron can be considered as a rigid body,[16] we thus set the O-O distances at 2 Å. This constrain implies the oxygen atoms to be link to each other in an octahedral environment and alows only octahedral rotations.

Furthermore, as shown with the simulated pole figures (figure 6), those intensities result in the convolution of several crystallographic plane contributions. According to the TEM analysis, the different orientations of the crystal in the film are perfectly known. In order to take into account these domains, we describe these orientations in the JANA2006 software using three twins matrices. One represents the four-axis symmetry loss along the [101] direction and corresponds to the description of the 90°-oriented domains. The two others are associated to the lost of the two-axes symmetry along the [100] and the [001] directions which creates 180°-oriented domains coming from the monoclinic symmetry.

In spite of the realistic obtained atomic positions reported in table 3 (right side), the usual accordance factors of the Rietvelt method are to high to consider the refinement results as valuable.[31] A new approach using the quantitative texture analysis and the MAUD software is currently under investigation in order to pursue the methodology. However, this work is a complete new approach to resolved fully the structure of an epitaxial thin film and underline promising results to correlate the structural analysis with the physical properties in the TMOs thin films.

V. CONCLUSIONS

In conclusion, we have demonstrated that it is possible to refined the structure of a $LaVO_3$ thin film from a laboratory X-ray diffraction analysis. In spite of the atomic positions refinement results, this study is a completely new approach to obtain structural insight of a strongly epitaxial thin film. The results are promising and further analysis are currently under investigation to pursue the methodology. Such analysis can be applied to many systems similar to $LaVO_3$.

VI. ACKNOWLEDGEMENTS

This research was financially supported by the LabEx EMC3. The authors would like to acknowledge L. Gouleuf for the cross-section preparation. HR thanks Pr B. Mercey and O. Perez for illuminating discussions ant their continuous encouragements during this work.

---

[1] G. Smolenskii, V. Bokov, J. Appl. Phys 35 (1964) 915.

[2] J. Wang, J. B. Neaton, H. Zheng, V. Nagarajan, S. B. Ogale, B. Liu, D. Viehland, V. Vaithyanathan, D. G. Schlom, U. V. Waghmare, N. A. Spaldin, K. M. rabe, M. Wuttig, R. Ramesh, Science 299 (2003) 1719.

[3] D. Dijkkamp, T. Venkatesan, X. D. Wu, S. A. Shaheen, N. Jisrawi, Y. H. Min-Lee, W. L. McLean, M. Croft, Appl. Phys. Lett. 51 (1987) 619.

[4] J. Hamet, B. Mercey, M. Hervieu, B. Raveau, Physica C 193 (1992) 465.

[5] M. Imada, A. Fujimori, Y. Tokura, Rev. Mod. Phys. 70 (1998) 1039.

[6] A. David, P. Boullay, R. V. K. Mangalam, N. Barrier, W. Prellier, Appl. Phys. Lett. 96 (2010) 221904.

[7] J. Rondinelli, N. A. Spalding, Adv. Mater. 23 (2011) 3363.

[8] J. Hubbard, Proc. Roy. Soc. 276 (1963) 238.

[9] P. A. Salvador, A.-M. Haghiri-Gosnet, B. Mercey, M. Hervieu, B. Raveau, Appl. Phys. Lett. 75 (1999) 2638.

[10] D. Chateigner, Combined Analysis, ISTE-WILEY, 2010.

[11] D. Remiens, L. Yang, F. Ponchel, J. F. Legier, D. Chateigner, G. Wang, X. Dong, Journal of Applied Physics 109 (2011) 114106.

[12] G. Leclerc, G. Poullain, R. Bouregba, D. Chateigner, Applied Surface Science 255 (2009) 4293 – 4297.

[13] R. S. Hassan, N. Viart, C. Ulhaq-Bouillet, J. Loison, G. Versini, J. Vola, O. Cregut, G. Pourroy, D. Muller, D. Chateigner, Thin Solid Films 515 (2007) 2943 – 2948.

[14] L.Lutterotti, D.Chateigner, S.Ferrari, J.Ricote, Thin solid film 450 (2004) 34.

[15] M. Moram, M. Vickers, Rep. Prog. Phys. (72) (2009) 036502.

[16] A. Glazer, Acta Cryst. B 28 (1972) 33842.

[17] A. Glazer, Acta Cryst. A 31 (1975) 756.

[18] S. J. May, J.-W. Kim, J. M. Rondinelli, E. Karapetrova, N. A. Spaldin, A. Bhattacharya, P. J. Ryan, Phys. Rev. B 82 (2010) 014110.

[19] H. Rotella, U. Luders, P.-E. Janolin, V. H. Dao, D. Chateigner, R. Feyerherm, E. Dudzik, W. Prellier, Phys. Rev. B 85 (2012) 184101.

[20] A. Vailionis, B. oschker, W. Siemons, E. P. Houwman, D. H. A. Blank, G. Rijnders, G. Koster, Phys. Rev. B 83 (2011) 064101.

[21] W. Lu, W. D. Song, K. He, J. Chai, C.-J. Sun, G.-M. Chow, J.-S. Chen, J. Appl. Phys. 113 (2013) 063901.

[22] P. Bordet, C. Chaillout, M. Marezio, Q. Huang, A. Santoro, S.-W. Cheong, H. Takagi, C. S. Oglesby, B. Batlogg, J. Solid State Chem. 106 (1993) 253.

[23] P. Boullay, A. David, W. C. Sheets, U. Luders, W. Prellier, H. Tan, J. Verbeeck, G. V. Tendeloo, C. Gatel, G. Vincze, , Z. Radi, Phys. Rev. B 83 (2011) 125403.

[24] Y. Hotta, H. Wadati, A. Fujimori, T. Susaki, H. Y. Hwang, Appl. Phys. Lett. 89 (2006) 251916.

[25] W. Sheets, P. Boullay, U. Luders, B. Mercey, W. Prellier, Thin Solid Films 517 (2009) 5130.

[26] E. J. Sonneveld, J. W. Visser, J. Appl. Cryst. 8 (1975) 1.

[27] J. Laugier, B. Bochu, Celref v3. www.inpg.fr

[28] C. J. Howard, H. T. Stokes, Acta Crys. B 54 (1998) 782.

[29] B. C. Server, Transtru.cryst.ehu.es

[30] V. Petricek, M. Dusek, L. Palatinus, Jana2006, the crystallographic computing system, institute of physics, praha, czech republic. (2006).

[31] H.-M. Rietveld, Acta Cryst. 22 (1967) 151.

Figures Captions:

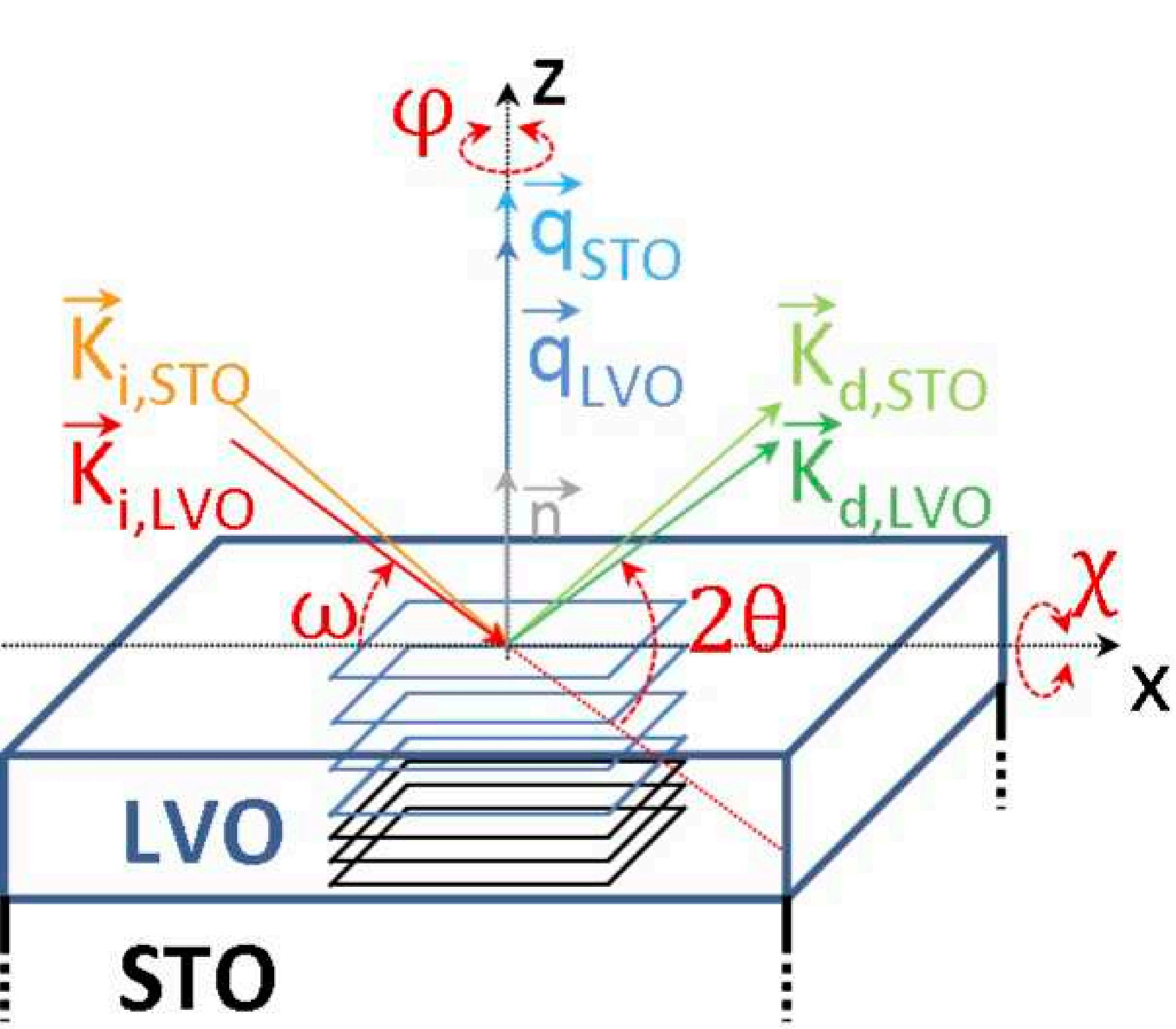
z
φ
$\vec{q}_{STO}$
$\vec{q}_{LVO}$
$\vec{k}_{i,STO}$
$\vec{k}_{i,LVO}$
$\vec{k}_{d,STO}$
$\vec{k}_{d,LVO}$
$\vec{n}$
ω
2θ
χ
x
LVO
STO

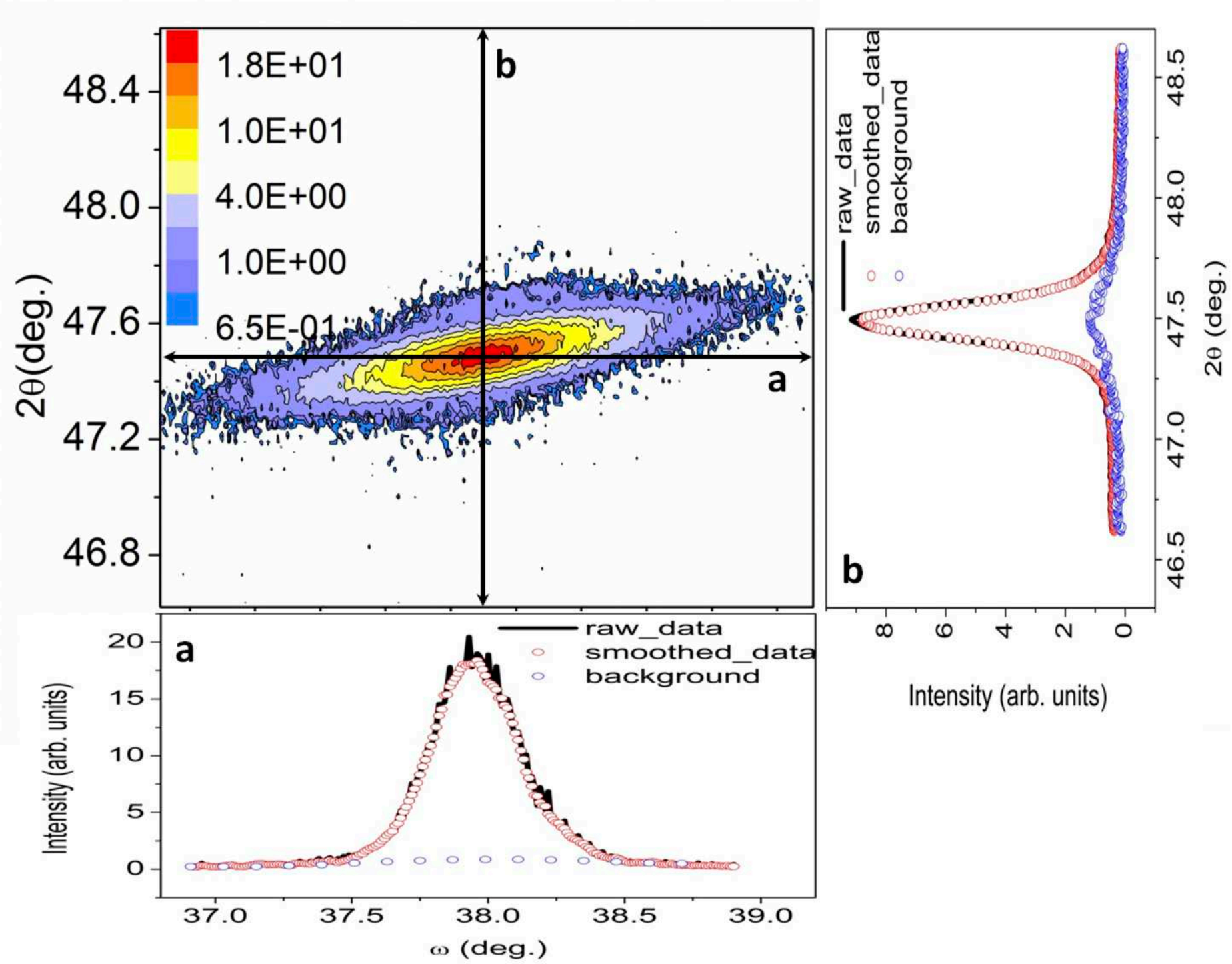
1.8E+01
1.0E+01
4.0E+00
1.0E+00
6.5E-01
b
a
2θ(deg.)
48.4
48.0
47.6
47.2
46.8
raw_data
smoothed_data
background
b
Intensity (arb. units)
2θ (deg.)
48.5
48.0
47.5
47.0
46.5
8
6
4
2
0
a
raw_data
smoothed_data
background
Intensity (arb. units)
20
15
10
5
0
37.0
37.5
38.0
38.5
39.0
ω (deg.)

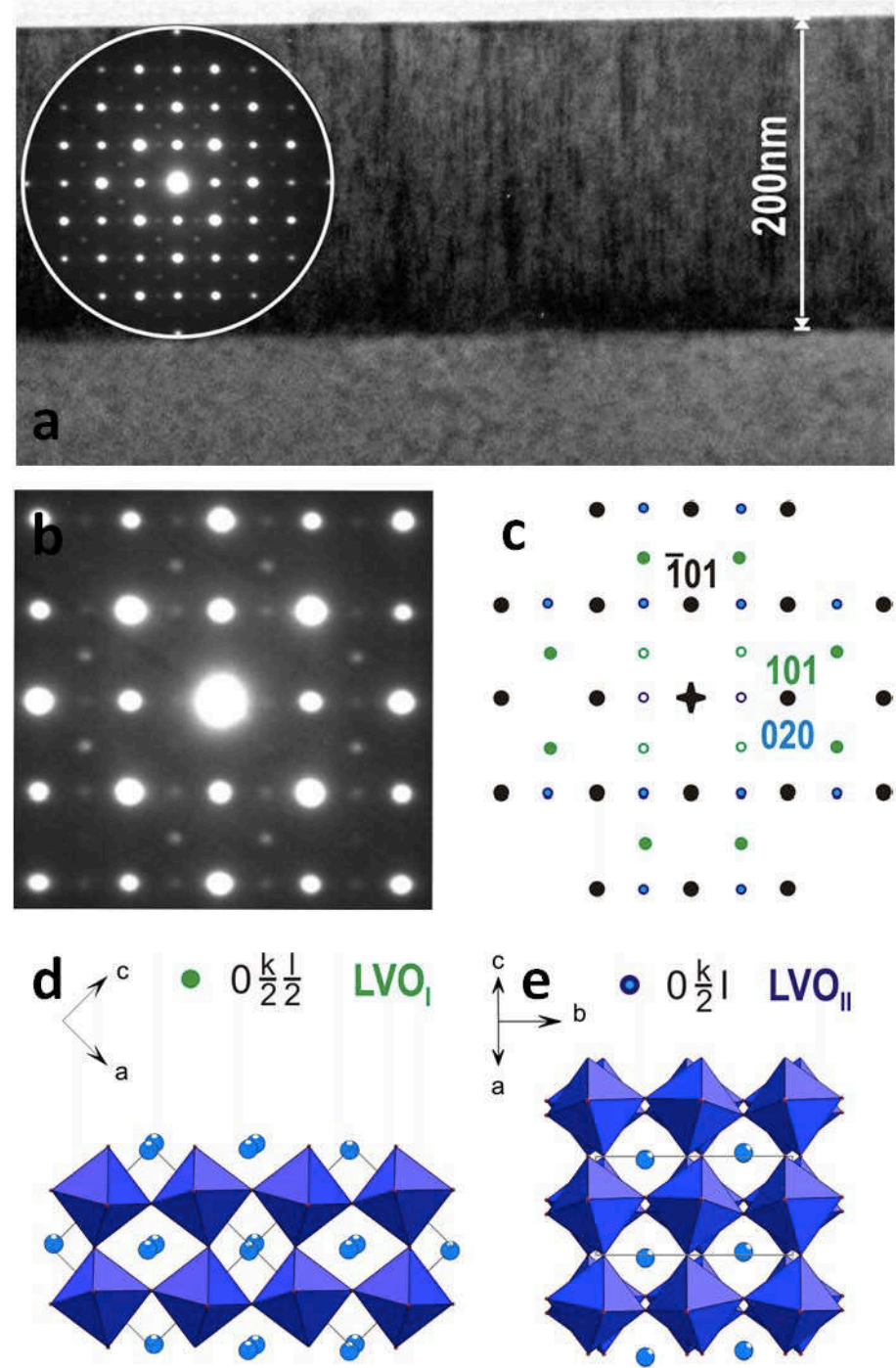
200nm
a
b
c
$\bar{1}01$
101
020
d
c
a
$0\frac{k}{2}\frac{l}{2}$
LVO_I
e
c
b
a
$0\frac{k}{2}l$
LVO_{II}

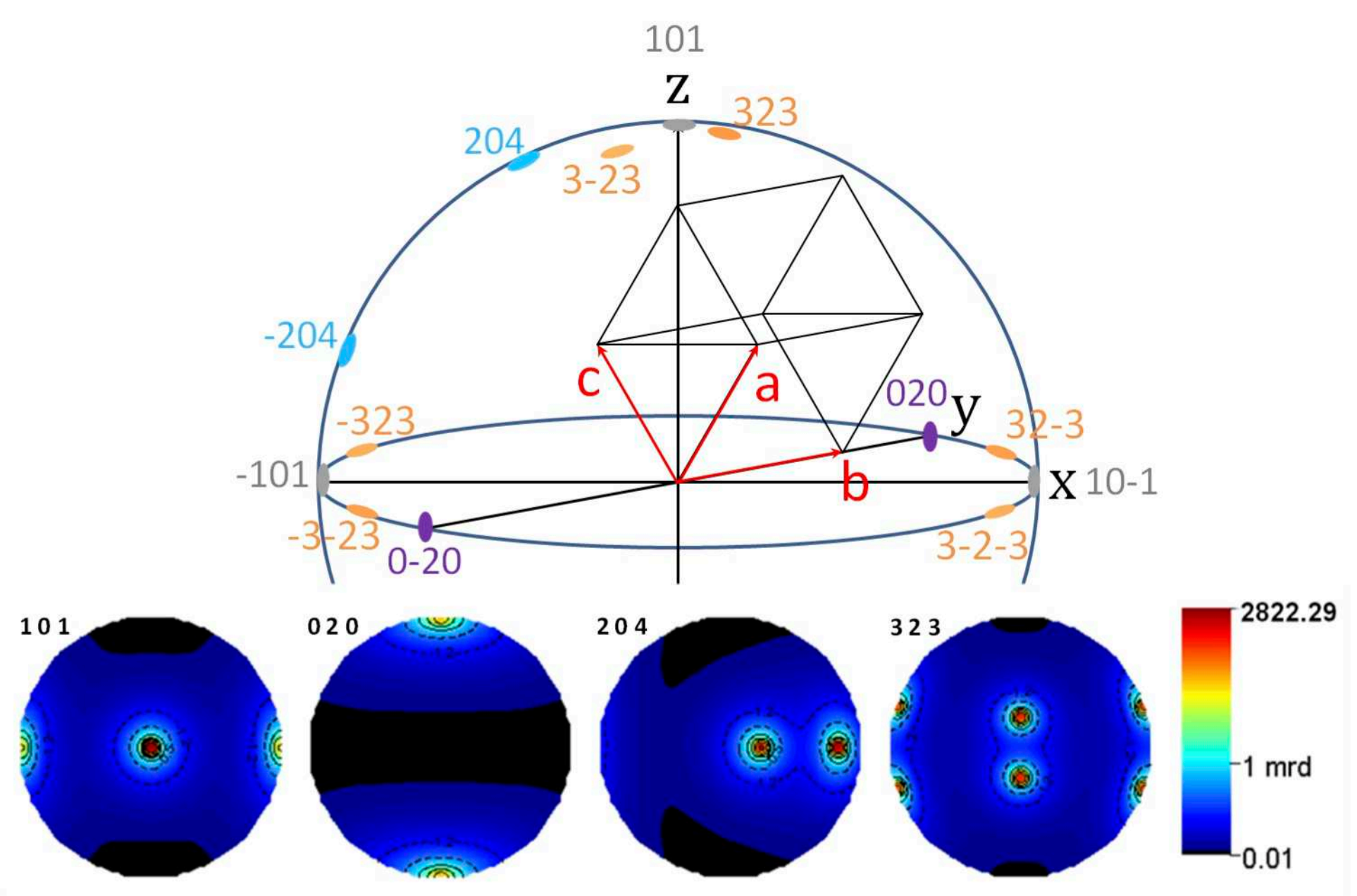
101
z
323
204
3-23
-204
c
a
020
y
-323
32-3
-101
x
10-1
b
-3-23
0-20
3-2-3
101
020
204
323
2822.29
1 mrd
0.01

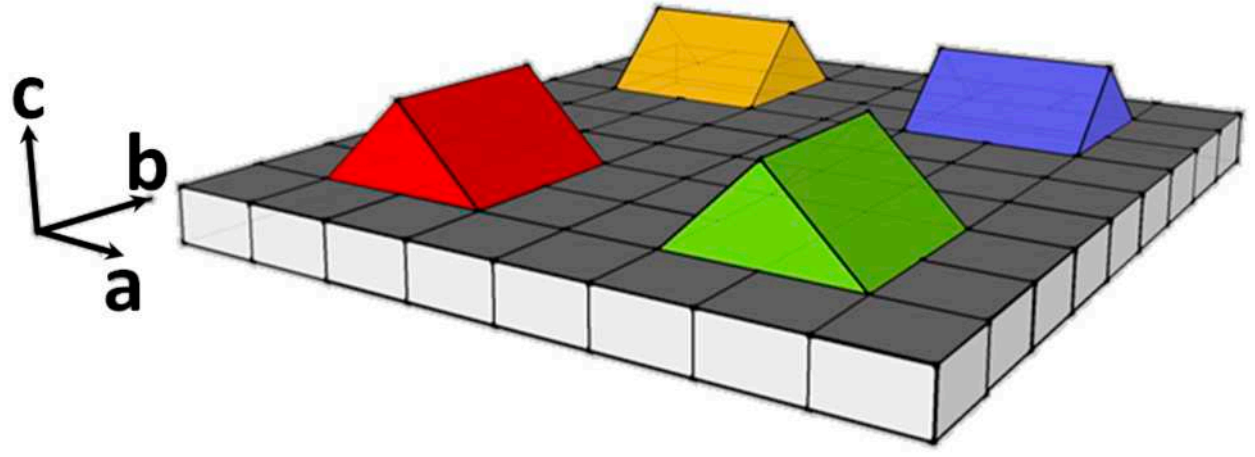
c
b
a

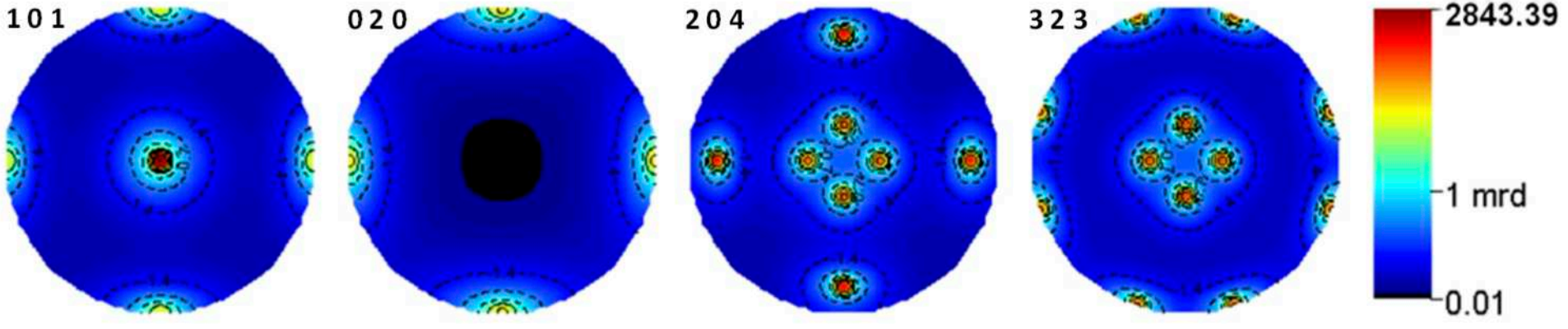
101
020
204
323
2843.39
1 mrd
0.01

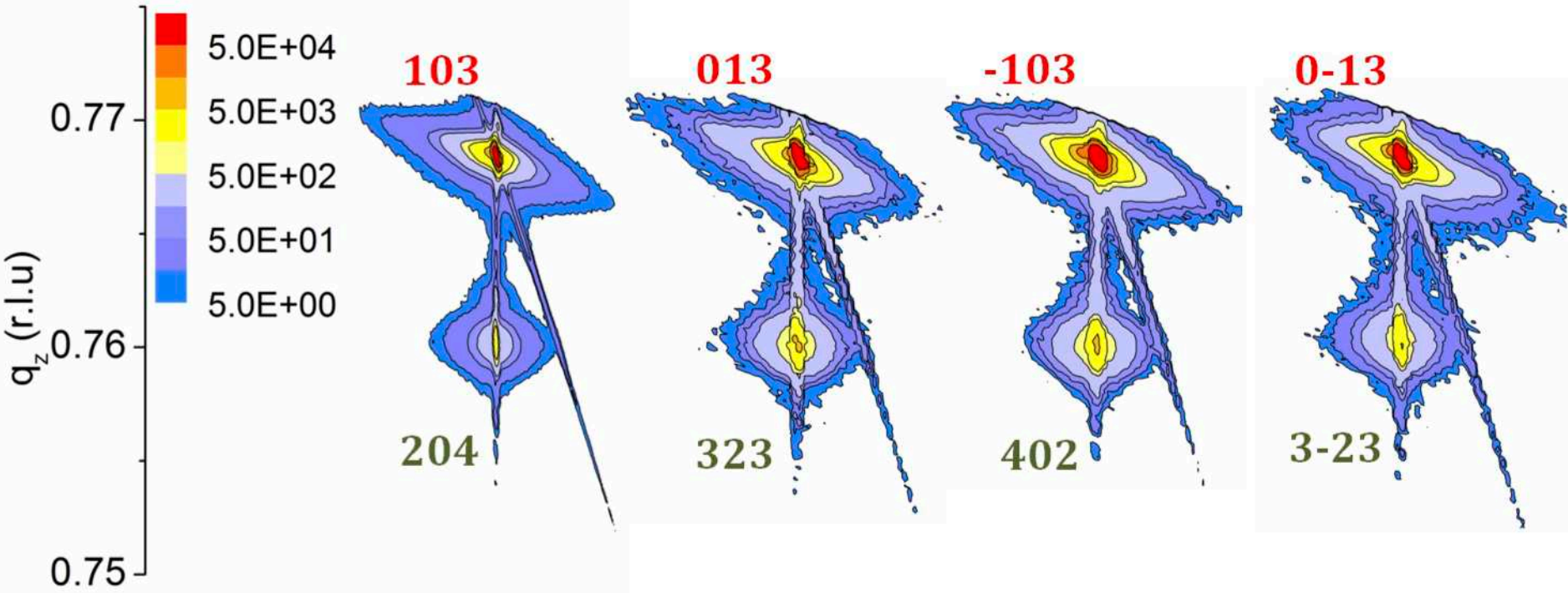
5.0E+04
5.0E+03
5.0E+02
5.0E+01
5.0E+00
0.77
0.76
0.75
q_z (r.l.u)
103
013
-103
0-13
204
323
402
3-23